Received 10 November 2018; revised 8 January 2019; accepted 22 January 2019. Date of publication 24 January 2019;
date of current version 1 March 2019. The review of this paper was arranged by Editor C. Surya.

Digital Object Identifier 10.1109/JEDS.2019.2895151

A Simple Analytic Modeling Method for SPAD Timing Jitter Prediction

FEIYANG SUN[1], YUE XU[1,2] (Member, IEEE), ZHONG WU[1], AND JUN ZHANG[1] (Member, IEEE)

1 College of Electronic and Optical Engineering, Nanjing University of Posts and Telecommunications, Nanjing 210023, China
2 National and Local Joint Engineering Laboratory of RF Integration and Micro-Assembly Technology, Nanjing University of Posts and Telecommunications, Nanjing 210023, China

CORRESPONDING AUTHOR: Y. XU (e-mail: yuex@njupt.edu.cn)

This work was supported in part by the National Natural Science Foundation of China under Grant 61571235 and Grant 61871231, in part by the Natural Science Foundation of Jiangsu Province of China under Grant BK20181379, in part by the QingLan Project of Jiangsu Province Colleges of China, and in part by the Graduate Research and Innovation Projects of Jiangsu Province of China under Grant SJCX18_0289.

ABSTRACT Timing jitter as a key performance of single-photon avalanche diode (SPAD) detectors plays a significant role in determining the fast temporal response behavior of the SPAD device. Nevertheless, few analytic models are developed to directly calculate the characteristic of timing jitter for its modeling difficulty. In this paper, we propose a simple analytic modeling method, which can predict the temporal response of SPADs, without using time-consuming Monte Carlo simulation. Model investigation incorporates avalanche current, avalanche buildup time, and jitter tail under different conditions. Furthermore, the key model parameters provided by Geiger mode technology computer-aided design simulation allow an accurate prediction on timing jitter. Analytical results indicate that for an SPAD device structure with a shallow P+/N-well junction in a 0.18-μm CMOS technology, the Gaussian peak response with about 110-ps full-width at half-maximum and the exponential jitter tail are in good agreement with the measured data, validating the accuracy, and feasibility of this modeling method.

INDEX TERMS Single photon avalanche diodes (SPADs), timing jitter, analytic model, jitter tail.

I. INTRODUCTION

Single photon avalanche diode (SPAD) detectors have attracted great interest in a variety of applications, such as Raman spectroscopy, photon counting technique, medical vision and 3D imaging in physical, chemical and biological fields, etc [1]–[3] due to high sensitivity and picosecond timing resolution. The temporal error interval of photon detection is termed timing jitter, which is a crucial indicator of the temporal response of SPADs. Recently, the rapid development of manufacturing and material technologies provides new insight into the performance improvements of timing jitter as well as photon detection efficiency (PDE) and dark count rate (DCR), etc. For instance, a mature SPAD device has been fabricated in advanced 40 nm Si technology, achieving a small timing jitter of 170 ps and a low DCR of 50 cps at 25 °C [4]. InGaAs/InP SPADs have been developed to acquire low crosstalk, high PDE of 20% at the near-infrared band, and very rapid temporal response [5], [6]. In addition, a backside-illuminated (BSI) 3D IC technology has also been adopted in SPADs to obtain maximum PDE of 21.9% at 660 nm and low timing jitter of 95 ps [7].

In order to attain high-speed and steady temporal response performance of SPADs at the design stage, a reliable physical model and a simple modeling method are in great demand for accurate timing jitter prediction. The Random Path Length (RPL) model was first proposed to study timing jitter properties [8], where the photon-assisted mechanism concerning avalanche spreading was investigated and the resistance of the neutral layer was also considered. Applying RPL-base physical models, the time-consuming Monte Carlo simulations were widely performed to estimate the temporal response characteristics. The analytic band [9] and full band [10] Monte Carlo simulations were used to study carrier transport and impact ionization, yet it brings high computational workload and complexity. Then, a simple Monte Carlo (SMC) model [11], [12] was developed to reduce computation time by considering less band structure details. Further, two main carrier scattering mechanisms, including effective intervalley phonon scattering and impact

ionization are incorporated in the SMC model to improve the accuracy of timing jitter modeling [13]. However, these SMC models still need complex Monte Carlo simulation to calculate the timing performance. Moreover, the exponential jitter tail modeling caused by the device-neutral regions is less studied, although the modeling methods of Gaussian temporal response in the device avalanche region are investigated in depth. Also, a computational method was presented to focus on the tail modeling [14], but the key model parameters, such as electron and hole ionization rates come from fitting theoretical or empirical values that are not correlated with the device structures and processes, which may reduce the accuracy of the model to some extent. Obviously, the previously reported models are not capable of establishing simple analytical expressions for accurate prediction of the overall timing jitter characteristics.

In this work, we propose a simple analytic modeling method to predict the temporal response of SPADs. Such an analytical statistical method by solving the two-dimensional avalanche current equation is adopted for modeling of Gaussian peak timing jitter for the first time. The diffusion and drift processes, as well as the recombination, are considered in the modeling of exponential jitter tail. Furthermore, the key model parameters such as electric field profiles, avalanche breakdown probability and ionization rate of carriers are provided by Geiger mode Technology Computer Aided Design (TCAD) simulation. As a consequence, the proposed modeling method is capable of establishing a predictable and accurate timing jitter model for a given device structure. It will be a promising candidate tool for the development of SPAD detectors with the improved performance.

II. PHYSICAL MECHANISM OF PHOTON DETECTION

As shown in Fig. 1(a), a typical shallow P+/N-well junction structure is used to illustrate the modeling method of timing jitter. This SPAD device mainly consists of a P+ implantation layer and an N-well that form a shallow depletion region and two neutral regions [15]. Under the excess bias state, once the photons are incident onto these three regions, the photonic carriers will be produced and spread over the entire detection area, as shown in Fig. 1(b) and (c), respectively. When the photons impinge onto the depletion region, because of the strong electric field in this region, the generated electron-hole pairs impact and ionize along the x-axis with a multiplication process, meanwhile they also diffuse in the y-z plane, eventually leading to the occurrence of avalanche events. Since the carries need a certain distance to accelerate and obtain enough energy before impact ionization occurs, the effect of dead space on avalanche, therefore, cannot be neglected [16].

However, the transportation mechanism of photo-generated carriers is different in neutral regions. In the N-well neutral region, the minority holes are generated and transport across the entire region along the x-direction. The avalanche could only be triggered after the carriers travel

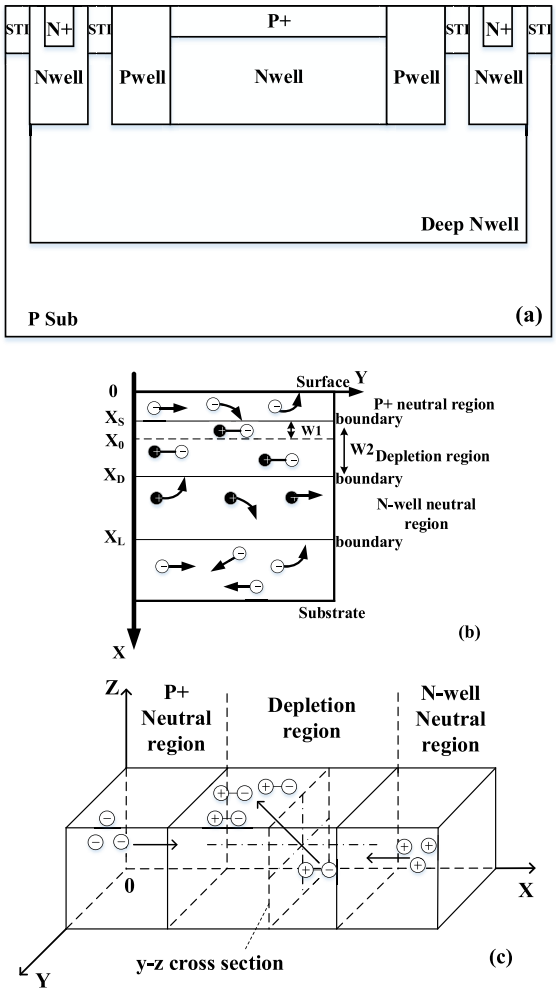

FIGURE 1. Schematic diagram of (a) P+/N-well SPAD device structure (b) carrier generation and (c) spreading mechanisms after absorbing photons.

across the boundary of the depletion region, leading to a time delay in detection. Thus, the temporal response of the neutral regions exhibits a shape of jitter tail. In principle, there is the same case in the P+ neutral region for the minority electrons. Whereas, most of the electrons are incapable of ionization due to high recombination rate. On the contrary, those electrons recombine with holes before they reach the avalanche region, causing this shallow photosensitive layer to contribute little to photon detection.

III. MODELING OF TIMING JITTER

Generally, the photon detection shows different timing performance in different detective regions. For one thing, the impact ionization and diffusion of the electron-hole pairs in the depletion region dominantly contribute to avalanche breakdown, inducing a fast peak response. For another, the drift and diffusion of the minority carriers in the neutral regions bring a delay for avalanche triggering. Therefore, the timing jitter modeling can be divided into two parts: a Gaussian peak of the depletion region plus an exponential

tail of the neutral regions as following

$$T_j \sim G(\mu, \sigma, t) + P_{neu}(t). \tag{1}$$

A. MODELING OF GAUSSIAN PEAK

In the depletion region, the photons inducing avalanche temporal response with a peak statistical feature can be evaluated by avalanche buildup time. According to the two-dimensional (2D) carrier spreading mechanism described above that electron-hole pairs drift and diffuse in the depletion region along two directions, the current continuity equation can be expressed by

$$\frac{dI}{dt} = \frac{I}{\tau} + D\nabla^2 I, \tag{2}$$

where τ is the multiplication time constant and D is the transverse diffusion coefficient.

The ionization multiplication is determined by τ, which reflects on the speed of the avalanche multiplication process. A simplified first-order expansion is given by [8]

$$\tau = \frac{\tau_i}{\frac{n}{F_b}(F_b - F_m)}, \tag{3}$$

in which, F_m is the maximum electric field of a PN junction, F_b is the electric field at the breakdown and n is the fitting value. The maximum electric field varies with the thickness of the depletion region and the reverse bias voltage. The fitting value n is related to the device structure and material, which is usually ranged from 1 to 4 for a Si-based device [17].

The intrinsic time τ_i is a response constant related to the device structure when carriers drift at saturated velocity. Referring to a correct quasistatic approximation analysis for semiconductor avalanche, the intrinsic time can be computed as [18]

$$\tau_i = \int_0^{W_2} \exp\left[-\int_x^{W_2} (\alpha_n - \alpha_p) dx'\right] \frac{dx}{|v_n| + |v_p|}. \tag{4}$$

Here, v_n and v_p are the electron and hole saturated velocity, α_n and α_p are the ionization coefficients for electrons and holes, respectively.

In order to solve the Eq. (2), we assume the total current flows along the electric field direction (x-direction), and set the current boundary conditions as follows: $I_y(0) = I_y(L_y) = 0$ and $I_z(0) = I_z(L_z) = 0$. Hence, an analytic avalanche current expression related to different y-z positions is yielded as

$$I(t) = \sum_{m,n=1}^{\infty} I_0 \exp\left\{\frac{t}{\tau} - Dt\left[\left(\frac{n\pi}{L_y}\right)^2 + \left(\frac{m\pi}{L_z}\right)^2\right]\right\} \sin\left(\frac{n\pi}{L_y} y\right) \sin\left(\frac{m\pi}{L_z} z\right), \tag{5}$$

where I_0 is the initial current, L_y and L_z are the width and the length of the depletion region, respectively.

By means of Eq. (5), the current variation at a position in the depletion region can be assessed. By extracting the time when the current reaches an avalanche threshold level of 100 μA at different positions on the y-z plane, a statistical distribution of avalanche buildup time is established. The next step is to extract meantime μ and standard deviation σ from this timing distribution for Gaussian peak modeling. Note that the standard deviation σ can be calculated by

$$\sigma = \sqrt{\frac{1}{N}\sum_{i=1}^{N}(t_i - \mu)^2}, \tag{6}$$

with N the number of samples and t_i the avalanche buildup time at a specified position.

The next step is to evaluate the temporal response dependent on PDE for obtaining the curve of timing jitter. The PDE is calculated to fit the peak of a Gaussian function as [19]

$$P_{DE} = \int_0^{W_2} \alpha e^{-\alpha x} P_{pair}(x) dx, \tag{7}$$

$$P_{pair}(x) = P_e(x) + P_h(x) - P_e(x)P_h(x), \tag{8}$$

with W_2 the thickness of the depletion region and α the absorption coefficient. $P_e(x)$ and $P_h(x)$ are the avalanche triggering efficiency initiated by the electron and hole at a position x, respectively. $P_{pair}(x)$ is the overall triggering efficiency that either an electron or hole triggers an avalanche event. Finally, the analytic formula of Gaussian peak response can be fitted by

$$G(\mu, \sigma, t) = P_{DE} e^{-\frac{(t-\mu)^2}{2\sigma^2}}. \tag{9}$$

B. MODELING OF EXPONENTIAL TAIL

The delay of photon detection in the neutral regions is responsible for a tail response. Similarly, the evaluation of photon detection efficiency for the jitter tail can be described by

$$P_{neu}(t) = E(t)P_e(x_S) + H(t)P_h(x_D), \tag{10}$$

where $H(t)$ is the hole flux density and $E(t)$ is the electron flux density. $P_e(x_S)$ and $P_h(x_D)$ are the efficiency that an electron and a hole triggers the avalanche at the edge of the depletion region, respectively (see Fig. 1 (b)). For a given device with a shallow P+/N-well junction in our work, the effect of the electron on the jitter tail can be neglected as the thin P+ neutral region is characterized by high electron recombination. The jitter tail is mainly determined by the temporal response of the N-well neutral region. Considering the diffusion and the drift as well as the recombination of holes, the carrier continuity equation becomes

$$\frac{\partial \Delta P}{\partial t} = D_p \frac{\partial^2 \Delta P}{\partial x^2} - \mu_p E \frac{\partial \Delta P}{\partial x} - \frac{\Delta P}{\tau_p}, \tag{11}$$

where D_p is the hole diffusion coefficient, μ_p is the hole mobility, E is the electric field and τ_p is the hole lifetime. It is worth noting that the drift component in Eq. (11) plays an important role in determining holes distribution despite a weak electric field in the neutral regions. With a well-defined boundary condition of the initial photon-generated

hole density N_P that highly depends on the photon absorption coefficient at a given wavelength, this equation is solved, obtaining the photon-generated hole concentration:

$$P(x,t) = \frac{N_P}{\sqrt{4\pi D_P t}} \exp\left[-\frac{(x-\mu_p E t)^2}{4D_P t} - \frac{t}{\tau_P}\right]. \quad (12)$$

Eq. (12) reflects on a process that the minority holes drift at a velocity of $\mu_P E$, diffuse in a concentration gradient and recombine with electrons. The hole flux density is further calculated according to the current density of the N-well neutral region, given by

$$H(t) = \frac{J(t)}{q} = \mu_p\left[P(x,t)E - \frac{k_0 T}{q}\frac{\partial P(x,t)}{\partial x}\right]. \quad (13)$$

Ultimately, after substituting Eq. (12) and Eq. (13) into Eq. (10), an analytic formula of the jitter tail with an exponential function can be obtained as

$$P_{neu} = H(t)P_h(x_D) = \mu_p\left(E + \frac{k_0 T(x-\mu_p E t)}{2qD_p t}\right)\frac{N_p}{\sqrt{4\pi t D_p}} \times \exp\left[-\frac{(x-\mu_p E t)^2}{4D_p t} - \frac{t}{\tau_p}\right]P_h(x_D). \quad (14)$$

Assuming that the lower boundary of the depletion region is the zero position, for a specific position x, the temporal response of the N-well neutral region can be estimated by Eq. (14).

IV. RESULTS AND DISCUSSION

A. TCAD DEVICE SIMULATION

By the aid of Geiger mode TCAD simulation, the accurate model parameters can be acquired. In term of the P+/N-well SPAD structure shown in Fig. 1(a), two-dimensional (2D) process simulation was performed using SILVACO Athena tool based on a standard 0.18μm CMOS process. Using the device structure obtained from this process simulation, 2D device simulation was operated with Shockley-Read-Hall recombination, low-field mobility, impact ionization, energy balance transport, and Geiger models, etc. For the P+/N-well SPAD device with a diameter of 15 μm, the simulated breakdown voltage is about 11.5 V at room temperature, which is very close to the measured result of 11.3 V. Fig. 2(a) shows the simulated 2D electric field profile across the whole device structure. A high electric field is found to be concentrated in the avalanche region. The doping profile in the depth direction is also illustrated in the inset of Fig. 2(a) where the junction depth of 0.3 μm is observed. Considering the effect of dead space, the ionization rates of electrons and holes are simulated at varying excess biases (V_{ex}). As Fig. 2(b) suggests, electrons contribute more ionizing events than holes. The electron ionization rate is almost twice that of the hole and the difference between them increases with the excess bias ranging from 0.3 V to 1.5 V.

Additionally, the electric field and avalanche triggering efficiency distributions in the entire detective region are

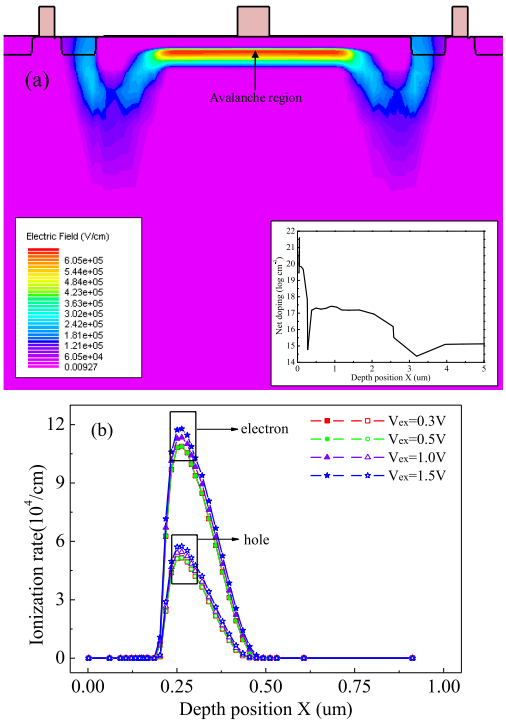

FIGURE 2. (a) Profiles of the 2D electric field and 1D doping level, and (b) distributions of electron and hole ionization rates at different excess bias voltages.

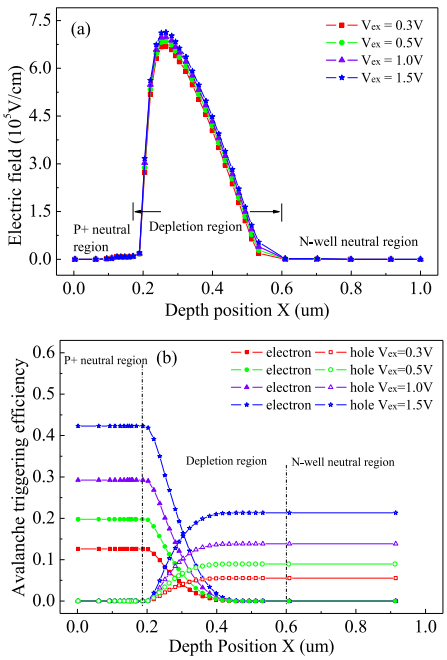

FIGURE 3. (a) The simulated electric field distribution and (b) avalanche triggering efficiency distribution in the entire detective area.

extracted by TCAD simulation. As depicted in Fig. 3(a), the electric field profiles exhibit a significant peak curve and the maximum level occurs at the center of the depletion

region. With the increase of the excess bias voltage from 0.3 V to 1.5 V, the peak electric field is enhanced by 4.4×10^4 V/cm. By comparison, the electric field in the neutral regions performs a uniform distribution and merely grows by 1200 V/cm. The avalanche triggering efficiency of electrons and holes in the entire detection area are presented in Fig. 3(b). The triggering efficiency of the electron remains constant in the P+ neutral region and presents a decreasing trend in the depletion region, nearly descending to zero in the N-well neutral region, while that of the hole suggests the opposite case. Crucially, the electron triggering efficiency at the upper boundary ($x = 0.18$ μm) and the hole triggering efficiency at the lower boundary ($x = 0.6$ μm) of the depletion region can be used for exponential tail modeling.

B. COMPUTATION AND VALIDATION

On the basis of the simulated ionization rates in the avalanche region (Fig. 2(b)), the intrinsic time constant is computed according to Eq. (4). Fig. 4 shows the intrinsic time response as a function of excess bias voltage. The decay of this temporal plot is found since the higher excess bias voltage can induce a swifter response. Furthermore, the multiplication time constant τ can be obtained at the different excessive biases. For instance, it is about 33 ps at 0.5 V excess bias with a fitting value n of 1.5.

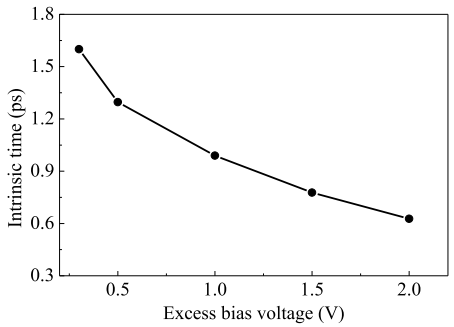

FIGURE 4. Intrinsic time response as a function of excess bias voltage.

Next, the multiplication process of the avalanche current in the depletion region is investigated. Fig. 5 presents the avalanche current at a position of the avalanche center region for different excess bias voltages, which are obtained by Eq. (5) with the average diffusion coefficient $D = 17$ cm^2/s [8]. For a higher excess bias voltage, the current rises more apparently as the stronger electric field provides a higher avalanche speed. The avalanche currents corresponding to 600 different photon impinging positions that are uniformly selected in 6 μm × 1 μm y-z plane of the depletion region, are assessed to establish a statistical distribution of avalanche buildup time. Fig. 6 shows one example of avalanche buildup time statistics in the depletion region at 0.5 V excess bias. Ultimately, the mean avalanche buildup time of about 410 ps and the standard deviation of 47 ps are extracted from this statistical distribution for Gaussian peak modeling.

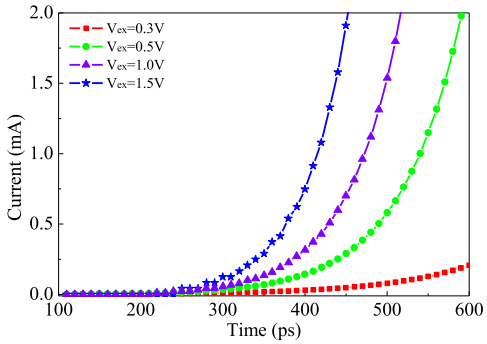

FIGURE 5. Multiplication response process of avalanche current at a position of the avalanche center region for different excess bias voltages ranging from 0.3 to 1.5 V.

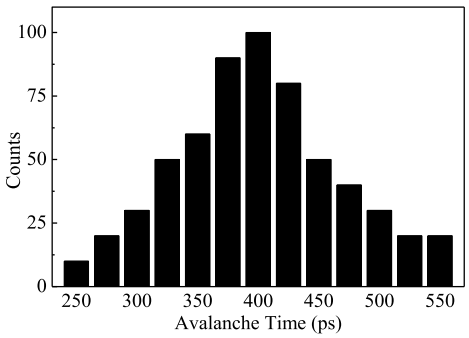

FIGURE 6. Avalanche buildup time statistics in the depletion region at 0.5 V excess bias.

The characteristics of jitter tail dependent on drift and diffusion distance as well as excess bias voltage are also evaluated. Here, the doping dependence of transportation parameters with the hole diffusion coefficient D_P of 13 cm^2/s, the hole mobility μ_P of 495 cm^2/ (V•s) and the hole lifetime τ_p of 10^{-7} s are used [14]. Fig. 7(a) illustrates the influence of different drift and diffusion distances on the temporal response characteristics of the N-well neutral region at an excess bias of 1.0 V. These temporal response curves are assumed to have the same initial PDE values, while different PDE values are presented at 0.5 ns due to the different decay rates under different position or excess bias conditions. Clearly, they exhibit an exponential decline in the tail. Meanwhile, a longer distance for which the minority carriers drift and diffuse is, a slower temporal response is. Fig. 7(b) shows the temporal response curves versus different excess bias voltages at a position of 0.2 μm distance from the lower boundary of the depletion region. As expected, when the higher overvoltage is applied, the swifter decay of temporal response is achieved. Whereas there is a special case when V_{ex} is 0.3 V, which is due to the fact that the recombination is mainly responsible for the relatively low PDE response value under the fairly weak electric field of less than 800 V/cm.

Fig. 8 illustrates the overall temporal response characteristics of the P+/N-well SPAD device by model calculation at

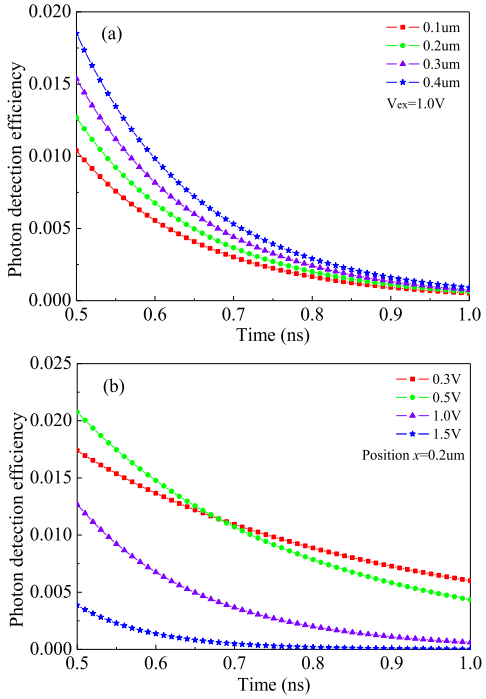

FIGURE 7. The temporal response in the N-well neutral region for (a) different drift and diffusion distances and (b) different excess bias voltages.

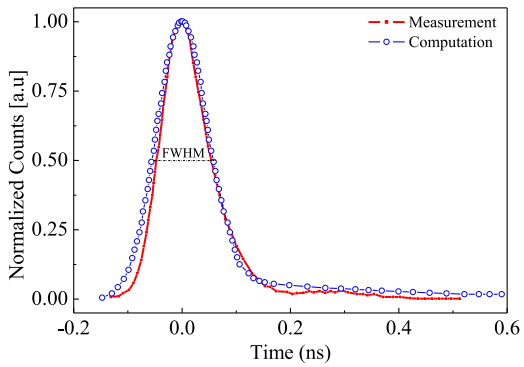

FIGURE 8. Comparison of timing jitter curve between model calculation results (hollow line) and experimental data (solid line) [20] for a P+/N-well device structure.

0.3 V excessive voltage. To validate the proposed model, the analytical results are compared with the reported measured data [20]. Although the compared SPAD device is fabricated in a different 0.18 μm standard CMOS technology [15], [20], it has the same P+/N-well structure (see Fig. 1(a)) and the same active diameter with our modeling device. Moreover, the two SPAD devices show almost the same breakdown voltage, indicating few differences in doping profiles between them, therefore there is good comparability between the measurement and computation results. It is clearly found that the analytical results agree well with the measured information. At the photon wavelength of 450 nm, the full-width at half-maximum (FWHM) from analytical results is about 110 ps, which is very close to the experimental value of 100 ps at the same excess bias of 0.3 V. Furthermore, the exponential tail of model calculation is also well matched with the exponential decay of the tested jitter tail. All the calculation results indicate the accuracy and feasibility of this modeling method.

V. CONCLUSION

A new analytic modeling method for exploring the complete timing jitter characteristics of SPADs is presented without using traditional time-consuming Monte Carlo simulation. The model investigates the avalanche current and avalanche buildup time and further adopts an analytical statistical method for modeling Gaussian peak response of the depletion region. The weak electric field dependence of carrier drift and diffusion as well as recombination in the neutral regions are also taken into account for jitter tail modeling. By solving the continuity equations which respectively reflect on bi-dimensional current variation and one-dimensional carrier transport mechanism, the analytic formulas of temporal response are derived. By means of the accurate model parameters obtained from the Geiger mode TCAD simulation, the timing jitter for a given SPAD structure can be accurately predicted. In summary, the computational timing jitter conforming to the experimental result suggests that this modeling method is reliable and instructive for the improvement of SPAD design.

REFERENCES

[1] J. A. Richardson, E. A. G. Webster, L. A. Grant, and R. K. Henderson, "Scaleable single-photon avalanche diode structures in nanometer CMOS technology," *IEEE Trans. Electron Devices*, vol. 58, no. 7, pp. 2028–2035, Jul. 2011.

[2] D. Bronzi, F. Villa, S. Tisa, A. Tosi, and F. Zappa, "SPAD figures of merit for photon-counting, photon-timing, and imaging applications: A review," *IEEE Sensors J.*, vol. 16, no. 1, pp. 3–12, Jan. 2016.

[3] L. Pancheri, N. Massari, and D. Stoppa, "SPAD image sensor with analog counting pixel for time-resolved fluorescence detection," *IEEE Trans. Electron Devices*, vol. 60, no. 10, pp. 3442–3449, Oct. 2013.

[4] S. Pellegrini *et al.*, "Industrialised SPAD in 40 nm technology," in *Proc. IEEE Int. Electron Devices Meeting (IEDM)*, Dec. 2017, pp. 16.5.1–16.5.4.

[5] X. Jiang *et al.*, "InP-based single-photon detectors and geiger-mode APD arrays for quantum communications applications," *IEEE J. Sel. Topics Quantum Electron.*, vol. 21, no. 3, pp. 5–16, May/Jun. 2015.

[6] N. Calandri, M. Sanzaro, L. Motta, C. Savoia, and A. Tosi, "Optical crosstalk in InGaAs/InP SPAD array: Analysis and reduction with FIB-etched trenches," *IEEE Photon. Technol. Lett.*, vol. 28, no. 16, pp. 1767–1770, Aug. 15, 2016.

[7] S. Lindner *et al.*, "A high-PDE, backside-illuminated SPAD in 65/40-nm 3D IC CMOS pixel with cascoded passive quenching and active recharge," *IEEE Electron Device Lett.*, vol. 38, no. 11, pp. 1547–1550, Nov. 2017.

[8] A. Spinelli and A. L. Lacaita, "Physics and numerical simulation of single photon avalanche diodes," *IEEE Trans. Electron Devices*, vol. 44, no. 11, pp. 1931–1943, Nov. 1997.

[9] E. Pop, R. W. Dutton, and K. E. Goodson, "Analytic band Monte Carlo model for electron transport in Si including acoustic and optical phonon dispersion," *J. Appl. Phys.*, vol. 96, no. 9, pp. 4998–5005, Nov. 2004.

[10] D. Dolgos, H. Meier, A. Schenk, and B. Witzigmann, "Full-band Monte Carlo simulation of high-energy carrier transport in single photon avalanche diodes with multiplication layers made of InP, InAlAs, and GaAs," *J. Appl. Phys.*, vol. 111, no. 10, pp. 1267–1288, May 2012.

[11] S. A. Plimmer, J. P. R. David, D. S. Ong, and K. F. Li, "A simple model for avalanche multiplication including dead space effects," *IEEE Trans. Electron Devices*, vol. 46, no. 4, pp. 769–775, Apr. 1999.
[12] X. Zhou, J. S. Ng, and C. H. Tan, "A simple Monte Carlo model for prediction of avalanche multiplication process in silicon," *J. Instrum.*, vol. 7, no. 8, pp. 451–455, Aug. 2012.
[13] J. D. Petticrew *et al.*, "Avalanche breakdown timing statistics for silicon single photon avalanche diodes," *IEEE J. Sel. Topics Quantum Electron.*, vol. 24, no. 2, Mar./Apr. 2018, Art. no. 3801506.
[14] A. Gulinatti *et al.*, "Modeling photon detection efficiency and temporal response of single photon avalanche diodes," in *Proc. SPIE*, vol. 7355, May 2009, Art. no. 73550X.
[15] I. Malass *et al.*, "Evaluation of size influence on performance figures of a single photon avalanche diode fabricated in a 180 nm standard CMOS technology," *Anal. Integr. Circuits Signal Process.*, vol. 89, no. 1, pp. 69–76, Oct. 2016.
[16] J. S. Ng *et al.*, "Effect of dead space on avalanche speed [APDs]," *IEEE Trans. Electron Devices*, vol. 49, no. 4, pp. 544–549, Apr. 2002.
[17] F. Laforce, "Low noise optical receiver using Si APD," in *Proc. SPIE*, vol. 7212, Feb. 2009, pp. 32–43.
[18] R. Kuvås and C. A. Lee, "Quasistatic approximation for semiconductor avalanches," *J. Appl. Phys.*, vol. 41, no. 4, pp. 1743–1755, Apr. 1970.
[19] Y. Xu, P. Xiang, and X. Xie, "A new modeling and simulation method for important statistical performance prediction of single photon avalanche diode detectors," *Semicond. Sci. Technol.*, vol. 31, no. 6, pp. 1–9, Jun. 2016.
[20] I. Malass, W. Uhring, J.-P. Le Normand, N. Dumas, and F. Dadouche, "A single photon avalanche detector in a 180 nm standard CMOS technology," in *Proc. IEEE New Circuits Syst. Conf.*, Aug. 2015, pp. 1–4.

FEIYANG SUN received the bachelor's degree from Guangling College, Yangzhou University, Yangzhou, China, in 2017.

He is currently pursuing the master's degree with the Nanjing University of Posts and Telecommunications, Nanjing, China.

YUE XU received the Ph.D. degree in microelectronics and solid-state electronics from Nanjing University, Nanjing, China, in 2012.

He is currently a Professor with the Nanjing University of Posts and Telecommunications, Nanjing.

ZHONG WU received the bachelor's degree from Jimei University, Xiamen, China, in 2017.

He is currently pursuing the master's degree with the Nanjing University of Posts and Telecommunications, Nanjing, China.

JUN ZHANG received the Ph.D. degree in microelectronics and solid-state electronics from the Nanjing University of Posts and Telecommunications, Nanjing, China, in 2018.

He is currently a Post-Doctoral Fellow with the Nanjing University of Posts and Telecommunications.